Aggregation kinetics and the nature of phase separation in two-dimensional dipolar fluids

Aggregation Kinetics and the Nature of Phase Separation in Two-Dimensional Dipolar Fluids

Peter D. Duncan and Philip J. Camp*

School of Chemistry, University of Edinburgh, West Mains Road, Edinburgh EH9 3JJ, United Kingdom

(Received 8 March 2006; published 6 September 2006)

The kinetics of aggregation in a monolayer of dipolar particles are studied using stochastic dynamics computer simulations. Transient concentrations of end defects (at low density) and Y-shaped defects (at high density) clearly exceed those at equilibrium. Although very large dipole moments are expected to disfavor such defects at equilibrium, it is found that the transient defect concentrations increase with increasing dipole moment. The results suggest that the conditions for defect-driven condensation—as proposed by Tlusty and Safran [T. Tlusty and S. A. Safran, Science **290**, 1328 (2000)]—could be met by kinetic trapping, giving rise to a metastable phase transition between isotropic fluid phases.

DOI: 10.1103/PhysRevLett.97.107202 PACS numbers: 75.50.Mm, 82.20.Wt, 82.70.Dd

The structure, phase behavior, and dynamics of strongly interacting, dipolar fluids present considerable challenges to soft-matter physics. The most common realization of a dipolar fluid is a ferromagnetic colloidal suspension, or ferrofluid. In the ideal case, this consists of spherical, homogeneously magnetized monodisperse particles with diameters ~ 10 nm, sterically stabilized and immersed in a nonpolar solvent. The resulting colloidal interactions are caricatured by the widely studied dipolar hard sphere fluid. Despite almost four decades of intensive experimental, theoretical, and simulation study [1,2], at least one outstanding question remains to be answered definitively: are point dipolar interactions alone sufficient to drive vapor-liquid phase separation? On the one hand, the Boltzmann-weighted, angle average of the dipole-dipole potential gives (to leading order) an isotropic, attractive pair potential that varies like $-1/r^6$, where r is the interparticle separation; this is expected to produce conventional condensation behavior [3]. On the other hand, simulations show that conventional condensation is preempted by strong aggregation, driven at low temperatures by the energetically favorable ''nose-to-tail'' conformation [4]. If phase separation occurs in 3D, then it is of a rather unusual nature; simulations suggest that the low-density phase mainly consists of chainlike aggregates, while the high-density phase resembles a network of interconnected segments [5]. One possible scenario involves a defect-mediated phase transition [6] in which the chains' defects are the singly connected particles at the chain ends (''end defects''), while the network's defects predominantly consist of particles with three near neighbors in a Y-shaped conformation (''Y defects'').

Recently, 2D dipolar fluids (with 3D magnetostatics) have received attention due to the possibility of directly imaging aggregation in thin films using cryogenic transmission electron microscopy [7–9]. The equilibrium structure [10,11] and dynamics [12] of 2D dipolar fluids have been studied in detail using computer simulations. At low density and low temperature (or large dipole moment), the dominant structural motifs are isolated chains and rings, while the high-density structure consists of a labyrinthine network of long chains (forming a ''disordered lamellar'' structure). There has never been any suggestion of a vapor-liquid phase transition in the 2D system, although end and Y defects *are* observed at equilibrium when the density and dipole moment are not too large; very large dipole moments disfavor Y defects because they are not ground-state conformations, while the excluded volume of Y defects means that the disordered lamellar structure is favored at very high densities. Note, however, that a transition between isolated and system-spanning clusters at low density has recently been characterized [13].

This Letter reports the first simulation study of the aggregation process in monolayers of strongly dipolar particles. Starting from equilibrated configurations of nonpolar particles, cluster formation is monitored after the dipoles are ''switched on''. The main findings are that high transient concentrations of end and Y defects are observed in aggregating systems with large dipole moments, and that these transient concentrations are always higher than the equilibrium values seen with smaller dipole moments. This suggests that the necessary conditions for defect-driven dipolar condensation might best be met by kinetically trapping transient, highly defective configurations. The results yield new insights on the properties of two-dimensional dipolar fluids, and, significantly, suggest a new strategy for realizing defect-driven condensations in the laboratory.

The system is modeled as a monolayer of monodisperse dipolar soft spheres. The interparticle potential is given by

$$u(\boldsymbol{r}, \boldsymbol{\mu}_1, \boldsymbol{\mu}_2) = 4\epsilon\left(\frac{\sigma}{r}\right)^{12} + \frac{\boldsymbol{\mu}_1 \cdot \boldsymbol{\mu}_2}{r^3} - \frac{3(\boldsymbol{\mu}_1 \cdot \boldsymbol{r})(\boldsymbol{\mu}_2 \cdot \boldsymbol{r})}{r^5}, \tag{1}$$

where ϵ is an energy parameter, σ is the sphere diameter, $\boldsymbol{\mu}_i$ is the dipole vector on particle i, $\boldsymbol{r}$ is the interparticle separation vector, and $r = |\boldsymbol{r}|$. To maintain a constant temperature in a physically relevant way, stochastic dynamics (as opposed to molecular dynamics) simulations

were performed according to the integrated Langevin equations [14]

$$\boldsymbol{r}_i(t+\delta t) = \boldsymbol{r}_i(t) + \frac{D_0^t}{k_B T}\boldsymbol{F}_i \delta t + \delta \boldsymbol{W}_i^t, \tag{2}$$

$$\hat{\boldsymbol{\mu}}_i(t+\delta t) = \hat{\boldsymbol{\mu}}_i(t) + \frac{D_0^r}{k_B T}\boldsymbol{T}_i \wedge \hat{\boldsymbol{\mu}}_i(t)\delta t + \delta \boldsymbol{W}_i^r \wedge \hat{\boldsymbol{\mu}}_i(t), \tag{3}$$

where $\boldsymbol{F}_i$ ($\boldsymbol{T}_i$) is the net force (torque) acting on dipole i at time t, $\hat{\boldsymbol{\mu}}_i = \boldsymbol{\mu}_i/\mu$ is a unit dipole orientation vector (renormalized after each time step), δt is the integration time step, and D_0^t (D_0^r) is the translational (rotational) diffusion constant at infinite dilution. The components of the 2D vector $\delta \boldsymbol{W}_i^t$ and the 3D vector $\delta \boldsymbol{W}_i^r$ were generated independently from Gaussian distributions subject to the conditions $\langle \delta \boldsymbol{W}_i^t \rangle = \langle \delta \boldsymbol{W}_i^r \rangle = 0$, $\langle \delta \boldsymbol{W}_i^t \cdot \delta \boldsymbol{W}_j^t \rangle = 4D_0^t \delta t \delta_{ij}$, and $\langle \delta \boldsymbol{W}_i^r \cdot \delta \boldsymbol{W}_j^r \rangle = 6D_0^r \delta t \delta_{ij}$. In this scheme the short-time inertial dynamics are suppressed, but this is appropriate because with large dipole moments, single-particle motions occur on time scales (in reduced units) of order 1 [12], while the collective motions of interest here are orders of magnitude slower.

In all simulations, the integration time step was $\delta t^* = 0.01$, where the reduced time is $t^* = t/\tau$ and $\tau = \sqrt{m\sigma^2/\epsilon}$. Results are presented for $N = 1024$ particles in an $L \times L$ simulation cell (with periodic boundary conditions) at densities $0.1 \le \rho^* = N\sigma^2/L^2 \le 0.5$, and with dipole moments $2 \le \mu^* = \sqrt{\mu^2/\epsilon\sigma^3} \le 2.75$; the temperature $T^* = k_B T/\epsilon = 1$ throughout. Characteristic diffusion constants were estimated from the (stick) Stokes-Einstein laws yielding $D_0^t = k_B T/3\pi\eta\sigma \simeq 4 \times 10^{-11}\ \mathrm{m^2\,s^{-1}}$ and $D_0^r = k_B T/\pi\eta\sigma \simeq 1 \times 10^6\ \mathrm{s^{-1}}$ for spherical particles with $\sigma = 10$ nm in a solvent of viscosity $\eta = 10^{-3}$ Pa s at temperature $T = 300$ K; the dimensionless quantities $D_0^t\tau/\sigma^2 = 0.004$ and $D_0^r\tau = 0.01$ were obtained using the mass of a 10 nm sphere with mass density $\sim 8000\ \mathrm{kg\,m^{-3}}$ (typical for iron or cobalt) and energy parameter $\epsilon = k_B T$. Self-assembly was initiated from configurations equilibrated with $\mu^* = 0$. For each density studied, five independent runs with different initial configurations were conducted and the results for each density were averaged, although the separate runs produced essentially identical results. The configurational temperatures associated with the positions and orientations of the particles were measured independently [15,16]. In each case the instantaneous configurational temperatures fluctuated about $T^* = 1$, with rms deviations of about 0.1, throughout the self-assembly process.

Figures 1(a) and 1(b) shows representative results for the different types of clusters that form in fluids with large dipole moments ($\mu^* = 2.75$), and at low and high densities ($\rho^* = 0.1$ and $\rho^* = 0.5$). Two neighboring particles are considered to belong to the same cluster if $u(\boldsymbol{r}, \boldsymbol{\mu}_1, \boldsymbol{\mu}_2) \le -0.6\mu^{*2}$ [17]. Clusters were classified as either chains

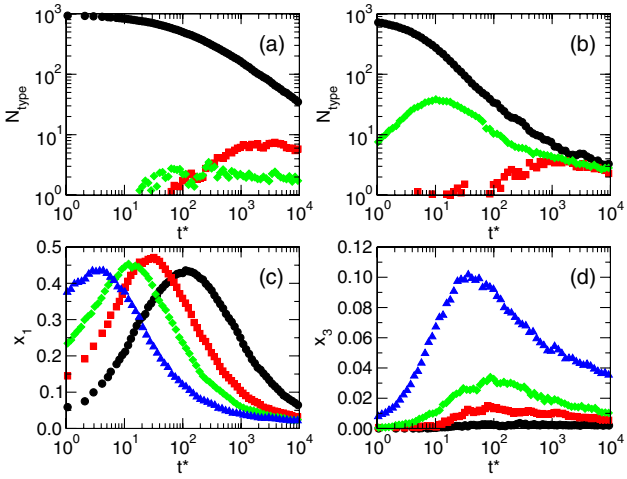

FIG. 1 (color online). Cluster properties in systems with $\mu^* = 2.75$: numbers of clusters at (a) $\rho^* = 0.1$ and (b) $\rho^* = 0.5$, classified as chains (black circles), rings (red squares), and X/Y defect clusters (green diamonds); (c) fraction of particles with one near neighbor and (d) fraction of particles with three near neighbors in fluids at densities $\rho^* = 0.1$ (black circles), $\rho^* = 0.2$ (red squares), $\rho^* = 0.3$ (green diamonds), and $\rho^* = 0.5$ (blue triangles).

(including monomers), rings, or "X/Y defect clusters" containing at least one particle with three (Y) or four (X) neighbors (particles with five or more neighbors were not observed). At low density ($\rho^* = 0.1$) the most common cluster is chainlike, followed by rings and then X/Y defect clusters. Chains are also favored at high density ($\rho^* = 0.5$), but X/Y defect clusters outnumber rings, and show a strong peak at $t^* \sim 10$; at equilibrium, the numbers of chains, rings, and X/Y defect clusters become comparable (and very small as the system undergoes almost complete aggregation). "Equilibrium" fluid structures at both densities are shown in Figs. 2(a) and 2(b). These two densities represent distinct regimes of aggregation behavior and will be considered separately.

Figure 3 shows the fractions of particles with n nearest neighbors, x_n, at time t during the aggregation processes at density $\rho^* = 0.1$ and with dipole moments $\mu^* = 2$, 2.25, 2.5, and 2.75. The monomer fraction—x_0—indicates that complete clustering is only established at equilibrium with $\mu^* \ge 2.5$. With $\mu^* \le 2.25$, x_1 (signaling end defects) increases to a finite equilibrium value. With larger dipole moments ($\mu^* \ge 2.5$) x_1 shows strong maxima at $t^* \sim 10^2$; note that these maxima exceed all of the equilibrium values seen at smaller dipole moments ($\mu^* \le 2.25$). The equilibrium values of x_2 indicate that extensive chaining (beyond dimers) occurs only when $\mu^* \ge 2.5$. At this low density, x_3 (signaling Y defects) is insignificant at all dipole moments; particles with four neighbors (X defects, not shown) are essentially absent. The lack of defect clusters suggests that aggregation proceeds by the sequential addition of particles or other small chains to the ends of existing chains, some of which fold up to form rings.

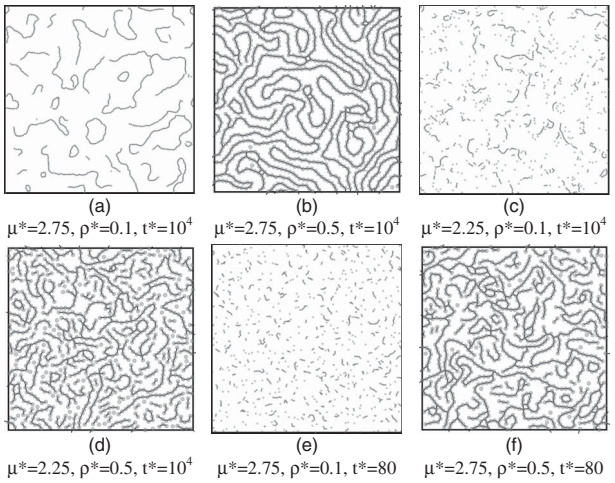

FIG. 2. Instantaneous configurations at various densities, dipole moments, and times. The black lines between particles denote "bonds" identified using the energy criterion.

Results for x_n at a high density of $\rho^* = 0.5$ are shown in Fig. 4. The equilibrium values of x_0 and x_2 show that the degree of chaining at equilibrium increases with increasing dipole moment, for obvious reasons. x_1 exhibits maxima at $t^* \sim 10$, while the equilibrium values decrease with increasing dipole moment, reflecting the energetic penalty of "dangling bonds". The behavior of x_3 depends sensitively on the dipole moment. With $\mu^* \leq 2.25$, x_3 increases from zero and plateaus at a value in the region of 0.05. At high density, even nonpolar particles are likely to have several near neighbors, some of which by chance may be oriented in such a way that when the dipoles are switched on, they cluster around a single particle to produce a Y defect. With small dipole moments, the energetic penalty of this configuration is not so severe, and the defect may

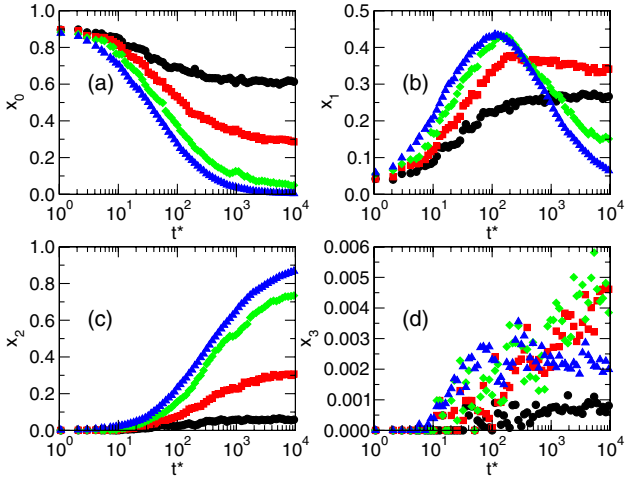

FIG. 3 (color online). Fractions of particles, x_n, with n neighbors during the aggregation process at density $\rho^* = 0.1$ and with dipole moments $\mu^* = 2$ (black circles), $\mu^* = 2.25$ (red squares), $\mu^* = 2.5$ (green diamonds), and $\mu^* = 2.75$ (blue triangles): (a) x_0; (b) x_1; (c) x_2; (d) x_3.

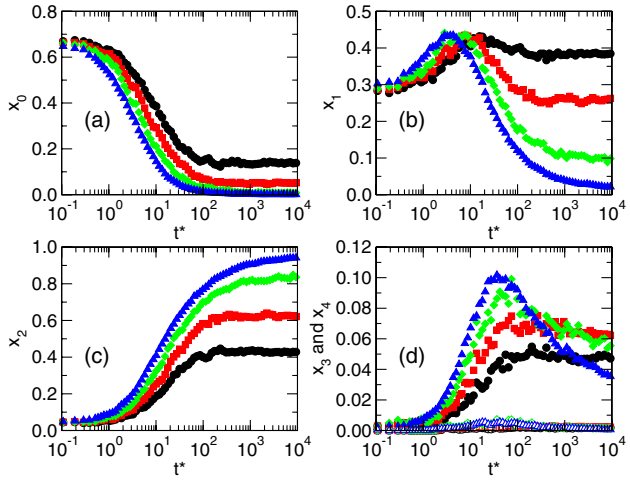

FIG. 4 (color online). Fractions of particles, x_n, with n neighbors during aggregation processes at density $\rho^* = 0.5$ and dipole moments $\mu^* = 2$ (black circles), $\mu^* = 2.25$ (red squares), $\mu^* = 2.5$ (green diamonds), and $\mu^* = 2.75$ (blue triangles): (a) x_0; (b) x_1; (c) x_2; (d) x_3 (filled symbols) and x_4 (open symbols).

persist at equilibrium. With larger dipole moments ($\mu^* \geq 2.5$), however, x_3 shows strong maxima at $t^* \sim 60$, and then tails off to values less than 0.05; significantly, the maxima are approximately two-thirds larger than the equilibrium values seen with smaller dipole moments. X defects (signaled by x_4) are at least an order of magnitude less numerous than Y defects, and are hence insignificant. These results suggest that larger dipole moments promote the initial formation of Y defects (as described above), but that since the associated Boltzmann weight of this configuration is not optimal, the Y defects "anneal out" to form the disordered lamellar phase as the fluid approaches equilibrium.

Defect-driven condensation involves a low-density phase rich in end defects, and a high-density phase rich in Y defects. It is therefore instructive to consider the equilibrium values of x_1, x_2, and x_3 at low density ($\rho^* = 0.1$) and high density ($\rho^* = 0.5$), as shown in Table I. With small dipole moments ($\mu^* \leq 2.25$), the end-defect concentrations at $\rho^* = 0.1$ are significant (~0.3), while the Y-defect concentrations at $\rho^* = 0.5$ are relatively small

TABLE I. Equilibrium ($t^* = \infty$) and transient values of x_1, x_2, and x_3 at densities of $\rho^* = 0.1$ and $\rho^* = 0.5$, and at various dipole moments.

		$\rho^* = 0.1$			$\rho^* = 0.5$		
μ^*	t^*	x_1	x_2	x_3	x_1	x_2	x_3
2	∞	0.29	0.08	<0.01	0.40	0.41	0.05
2.25	∞	0.32	0.32	<0.01	0.28	0.60	0.06
2.5	∞	<0.15	>0.73	<0.01	<0.10	>0.85	<0.04
2.75	∞	<0.06	>0.87	<0.01	<0.02	>0.94	<0.02
2.5	100	0.40	0.16	<0.01	0.17	0.71	0.09
2.75	80	0.43	0.19	<0.01	0.14	0.74	0.10

(~0.05). With larger dipole moments ($\mu^* \geq 2.5$) the equilibrium end-defect and Y-defect concentrations become negligible. (With these large dipole moments, the approach to equilibrium is extremely slow, hence the inequality signs in Table I). This provides an explanation of why an equilibrium defect-driven condensation has not been observed in 2D dipolar fluids: at all dipole moments (or temperatures) there are insufficient concentrations of end defects and Y defects in the low-density and high-density states, respectively.

Transient defect concentrations with $\mu^* = 2.5$ and $\mu^* = 2.75$ are also reported in Table I. In each case times are selected roughly halfway in between the positions of the peaks in x_1 at low density [Fig. 3(b)] and x_3 at high density [Fig. 4(d)]. The key point is that the transient end-defect concentration (at low density) and Y-defect concentration (at high density) are simultaneously greater than the equilibrium values with smaller dipole moments. In addition, the transient end-defect concentrations in the high-density fluid are much smaller with $\mu^* \geq 2.5$ than are the equilibrium concentrations with $\mu^* \leq 2.25$. These findings can be made more tangible by looking at simulation snapshots. Figures 2(c) and 2(d) shows equilibrium structures with $\mu^* = 2.25$, and $\rho^* = 0.1$ and $\rho^* = 0.5$; these are to be compared with the *transient* configurations at the same densities, but with $\mu^* = 2.75$ [Figs. 2(e) and 2(f)].

Thus far, only two densities have been considered, but in Figs. 1(c) and 1(d) are shown x_1 and x_3 for fluids with dipole moment $\mu^* = 2.75$, and at a selection of densities in the range $0.1 \leq \rho^* \leq 0.5$. x_1 peaks earlier and x_3 shows stronger maxima as the density is increased, due to the particles being in closer proximity when the dipoles are first switched on. It is clear that the extremes of this density range correspond to quite distinct regimes of aggregation behavior.

In summary, at low density aggregation proceeds through the formation of chains, some of which go on to form rings; above a critical dipole moment (in the range $\mu_c^* = 2.25$–2.5) transient concentrations of end defects exceed the equilibrium values observed with smaller dipole moments. At high density, increasing the dipole moment leads to a reduction (enhancement) of the equilibrium (transient) Y-defect concentration. When $\mu^* > \mu_c^*$, there is a time window in which the concentrations of end defects in the low-density fluid ($\rho^* \sim 0.1$) and Y defects in the high-density fluid ($\rho^* \sim 0.5$) are simultaneously close to their maximal values. Such defects are precisely those implicated in the defect-driven condensation of dipolar fluids [6]. It might therefore be possible to access a metastable phase separation, even in thin films where no equilibrium transition is expected, through kinetic stabilization of end defects (characterizing the low-density phase) and Y defects (characterizing the high-density phase). For instance, in ferrofluids a rapid temperature quench could freeze the carrier solvent and trap transient defects. Alternatively, the addition of a strong short-range isotropic attraction (e.g., chemically, or with added polymer to induce depletion forces) might stabilize defects. In this scenario, the long-range dipolar interactions drive the initial formation of small clusters with end and Y defects, while the short-range isotropic attractions preclude subsequent reorganization into the equilibrium structures. The relative ease with which 2D dipolar systems can be imaged directly may offer the best hope yet of realizing such a transition in the laboratory.

We thank Gren Patey, Sam Safran, Paulo Teixeira, and Tsvi Tlusty for correspondence, and the School of Chemistry at the University of Edinburgh for support to P. D. D.

*Electronic address: philip.camp@ed.ac.uk

[1] P. I. C. Teixeira, J. M. Tavares, and M. M. Telo da Gama, J. Phys. Condens. Matter **12**, R411 (2000).
[2] C. Holm and J.-J. Weis, Curr. Opin. Colloid Interface Sci. **10**, 133 (2005).
[3] P. G. de Gennes and P. A. Pincus, Phys. Kondens. Mater. **11**, 189 (1970).
[4] J. J. Weis and D. Levesque, Phys. Rev. Lett. **71**, 2729 (1993).
[5] P. J. Camp, J. C. Shelley, and G. N. Patey, Phys. Rev. Lett. **84**, 115 (2000).
[6] T. Tlusty and S. A. Safran, Science **290**, 1328 (2000).
[7] V. F. Puntes, K. M. Krishnan, and A. P. Alivisatos, Science **291**, 2115 (2001).
[8] K. Butter, P. H. H. Bomans, P. M. Frederik, G. J. Vroege, and A. P. Philipse, Nat. Mater. **2**, 88 (2003).
[9] M. Klokkenburg, R. P. A. Dullens, W. K. Kegel, B. H. Erné, and A. P. Philipse, Phys. Rev. Lett. **96**, 037203 (2006).
[10] J. M. Tavares, J. J. Weis, and M. M. Telo da Gama, Phys. Rev. E **65**, 061201 (2002).
[11] J.-J. Weis, J. Phys. Condens. Matter **15**, S1471 (2003).
[12] P. D. Duncan and P. J. Camp, J. Chem. Phys. **121**, 11 322 (2004).
[13] J. M. Tavares, J. J. Weis, and M. M. Telo da Gama, Phys. Rev. E **73**, 041507 (2006).
[14] R. B. Jones and F. N. Alavi, Physica A (Amsterdam) **187**, 436 (1992).
[15] O. G. Jepps, G. Ayton, and D. J. Evans, Phys. Rev. E **62**, 4757 (2000).
[16] A. A. Chialvo, J. M. Simonson, P. T. Cummings, and P. G. Kusalik, J. Chem. Phys. **114**, 6514 (2001).
[17] This energy cutoff captures likely conformations for neighboring dipoles, either in chains or in defect environments, and was determined on the basis of energy calculations for a number of different minimum-energy conformations. Cluster assignments were validated by direct inspection of the simulation configurations.